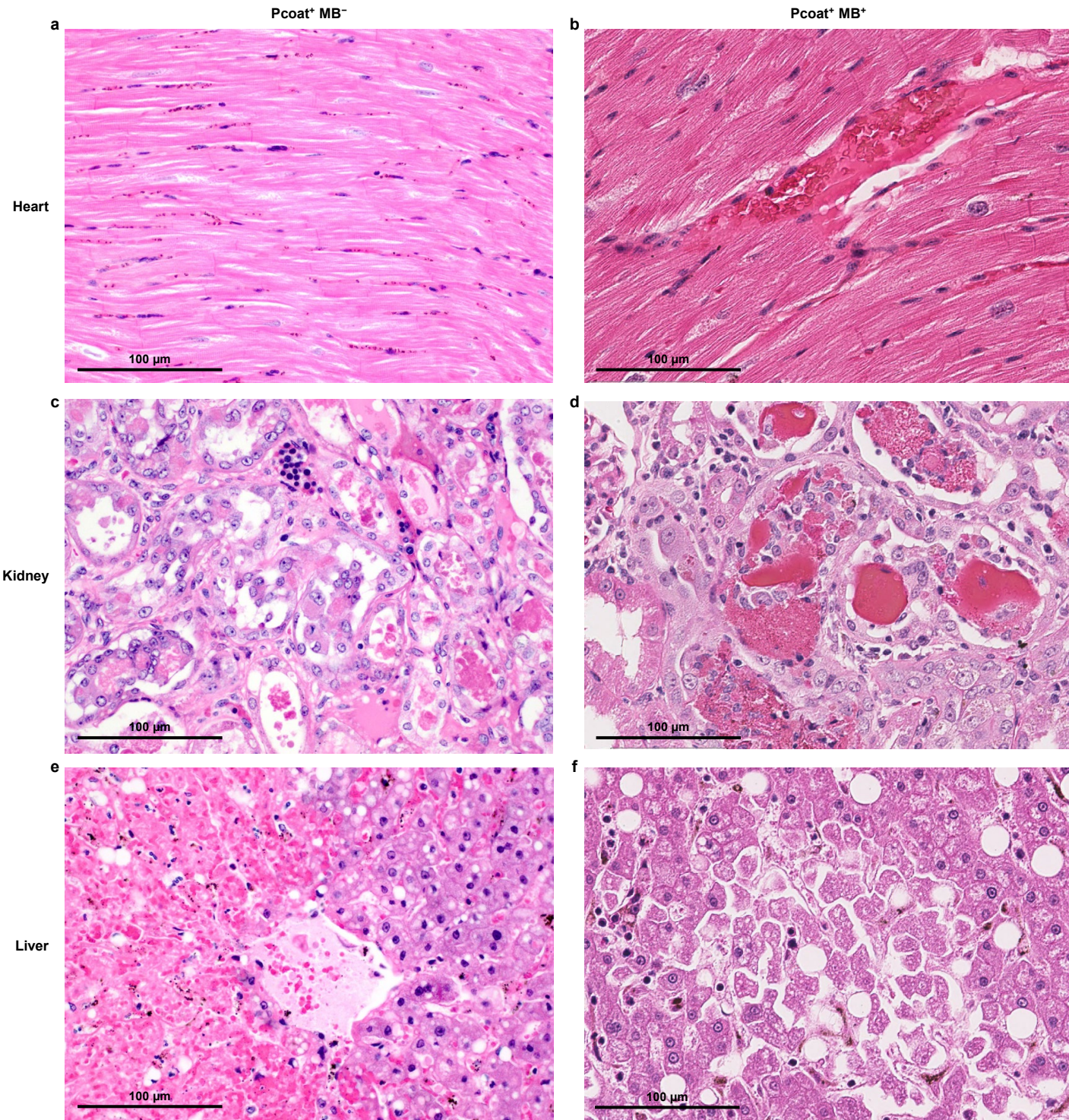
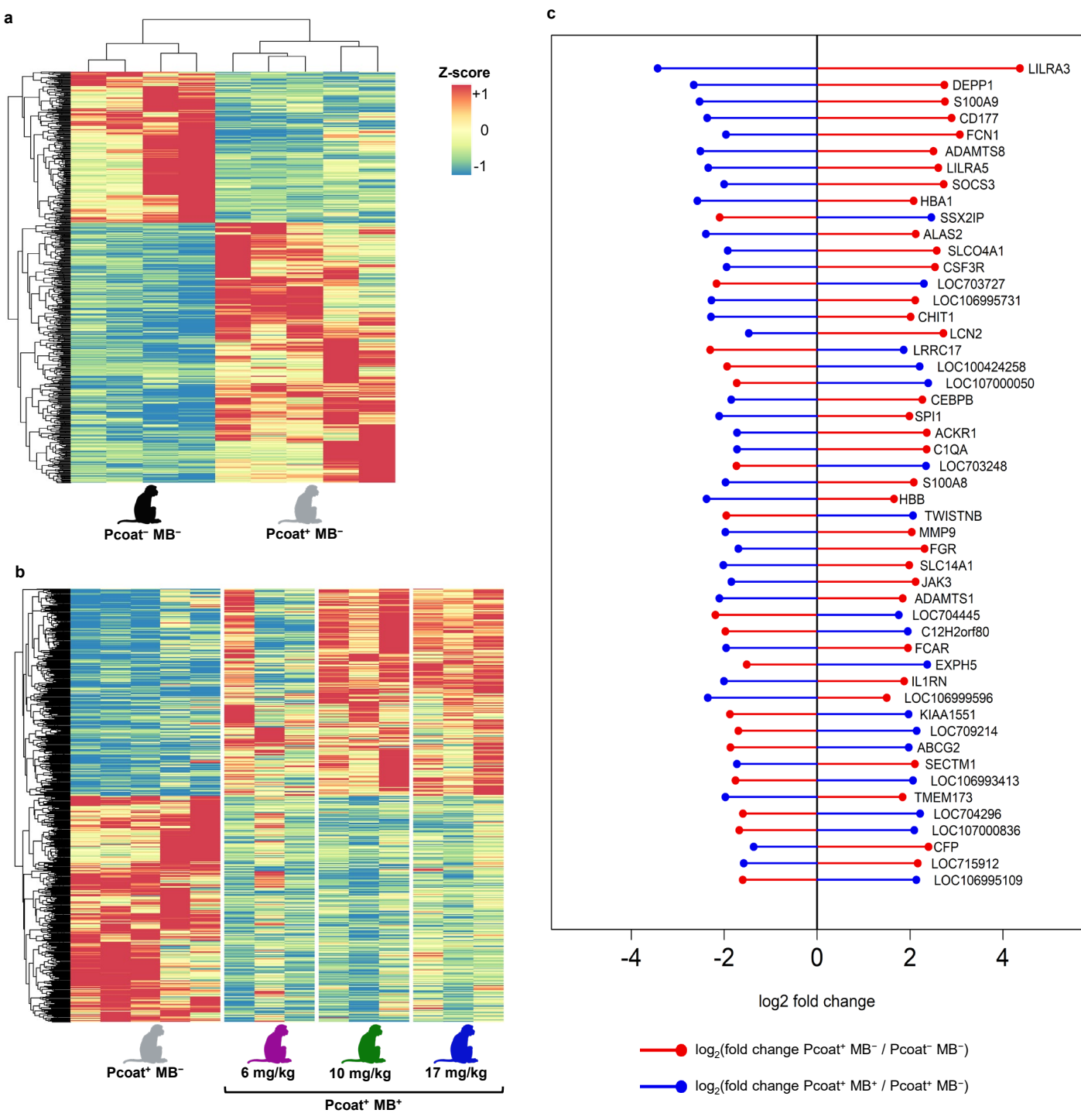


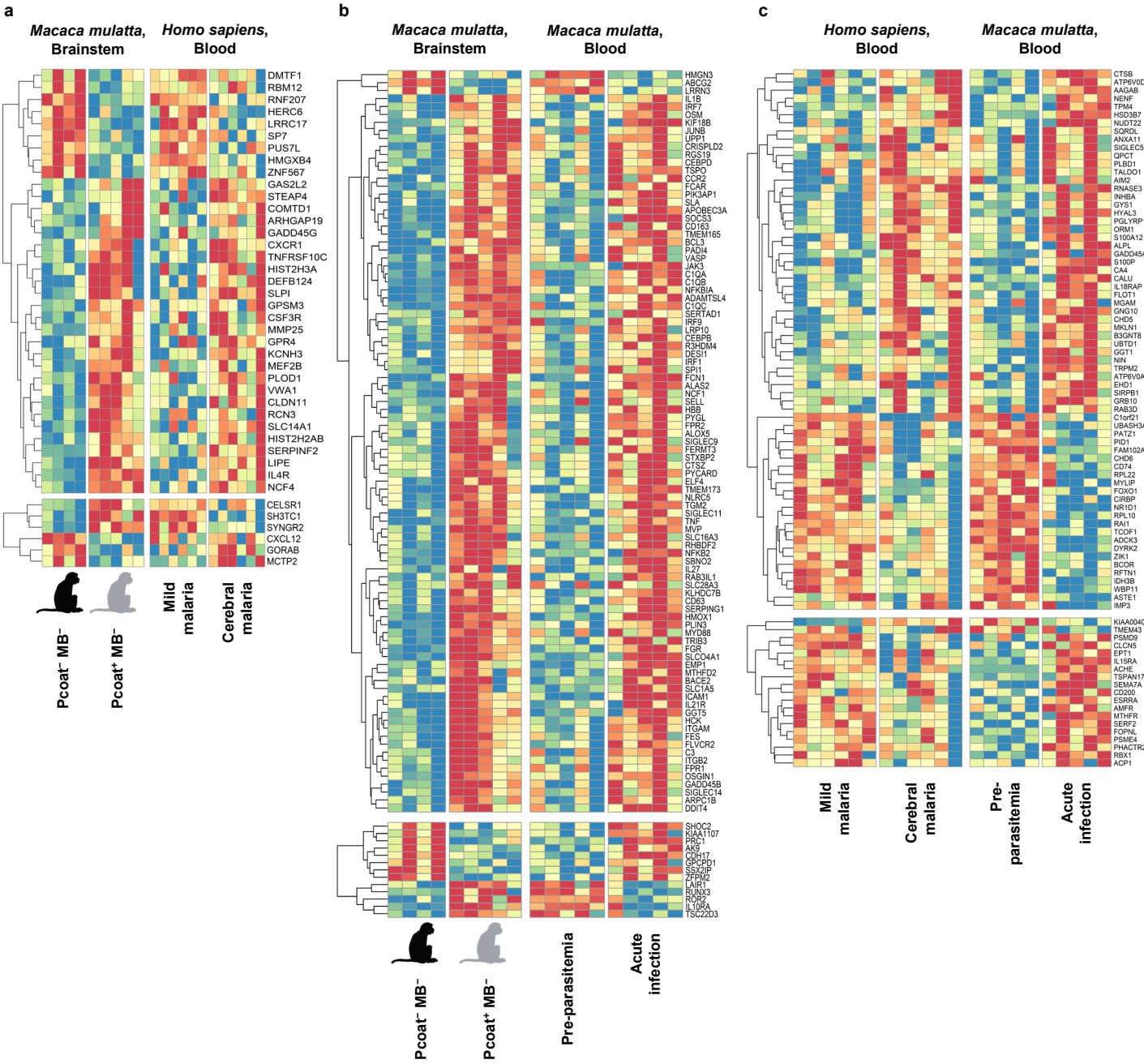
Supplementary Figure 1. Hierarchical clustering and principal component analysis of gene expression in different tissues during *P. coatneyi* infection. **a** Hierarchical clustering of RNA-seq samples using Jensen-Shannon divergence as the distance metric. Principal component analysis of RNA-seq samples in **b** heart, **c** kidney and **d** liver.



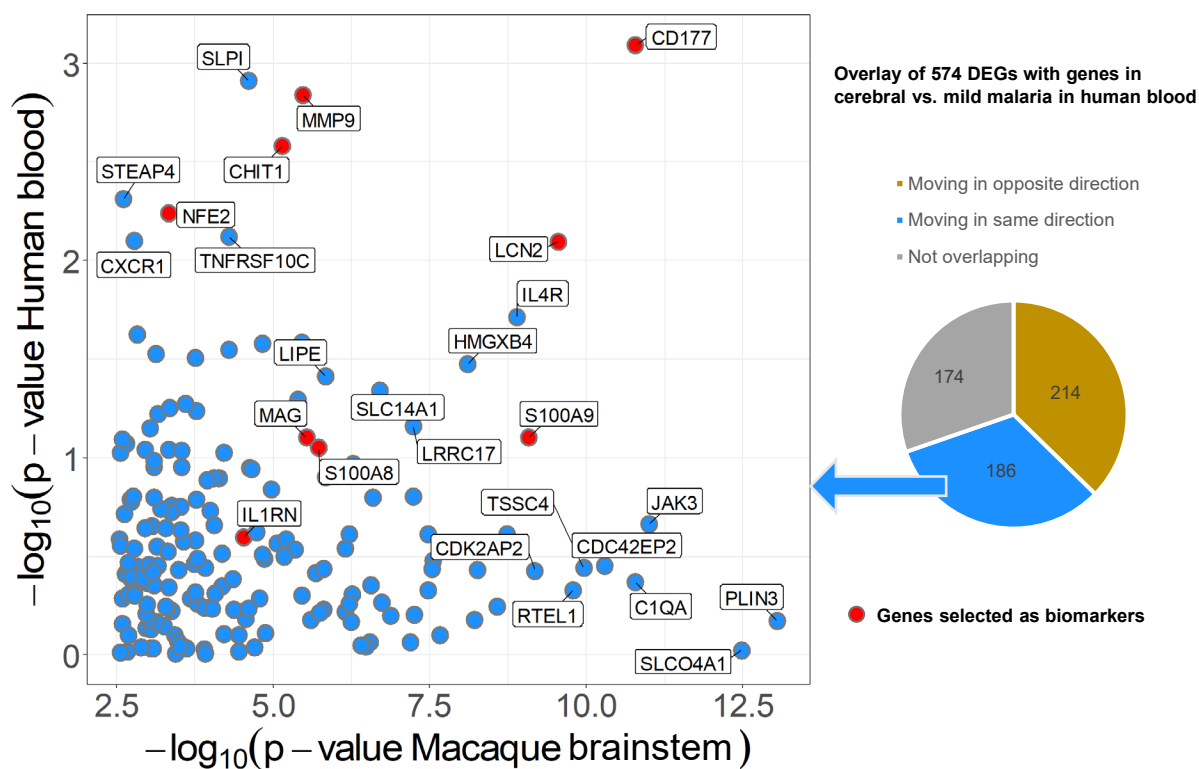
Supplementary Figure 2. Histological evidence of *P. coatneyi* induced pathology in heart, kidney and liver via H&E staining. **a** Heart (Pcoat⁺ MB⁻): There is marked congestion and sequestration of interstitial microvasculature with infected RBCs containing abundant hemozoin. **b** Heart (Pcoat⁺ MB^{17mg/kg}): Multifocally, the nuclei of cardiomyocytes are markedly enlarged (karyomegaly). Occasionally cardiomyocytes and interstitial pericytes contain golden brown granular pigment interpreted to be ceroid or hemosiderin. **c** Kidney (Pcoat⁺ MB⁻): This photomicrograph illustrates severe tubular epithelial degeneration and necrosis with hemoglobin casts. **d** Kidney (Pcoat⁺ MB^{17mg/kg}): There is evidence of marked tubular hemoglobin casts, proteinosis, cellular casts, epithelial degeneration, necrosis and regeneration, and histiocytic and lymphoplasmacytic interstitial nephritis. **e** Liver (Pcoat⁺ MB⁻): Hepatocellular dissociation multifocal to coalescing with abundant infected erythrocytes and hemozoin pigment accumulation in interstitial and sinusoidal spaces. **f** Liver (Pcoat⁺ MB^{6mg/kg}): Multifocally there is mild centrilobular coagulative necrosis, with hepatocellular dissociation admixed with frequent histiocytes containing intracytoplasmic brown pigment interpreted to be hemosiderin. Scale bar represented 100 µm. MB-treated photomicrographs are representative of pathology observed across the three animals in each dosage group. Pathology in Pcoat⁺ MB⁻ is supported by extensive retrospective and prospective studies (Lombardini ED et al., 2015; Lombardini ED, 2017).



Supplementary Figure 3. The effect of methylene blue treatment on gene expression for DEGs in the brainstem. **a** Heatmap of 801 DEGs modulated by infection in the brainstem. Created in BioRender. Malleret, B. (2025) <https://BioRender.com/lee54qw>. **b** Heatmap of 1709 DEGs modulated by methylene blue treatment in the brainstem of infected macaques. Created in BioRender. Malleret, B. (2025) <https://BioRender.com/lee54qw>. **c** The top 50 genes modulated by methylene blue treatment.

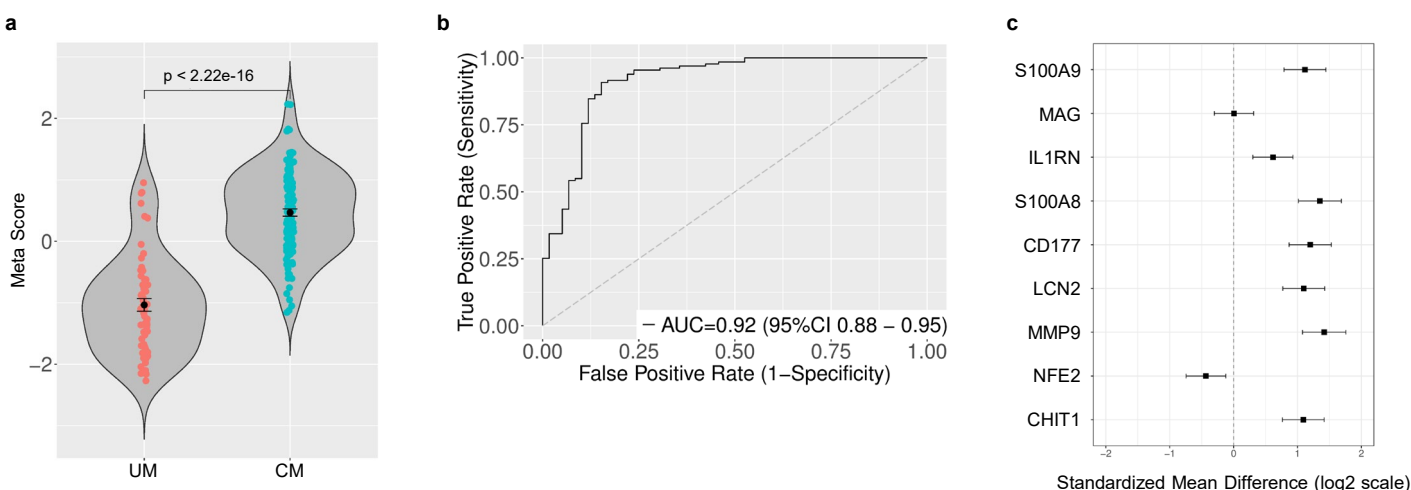


Supplementary Figure 4. Heatmap of overlapping genes during *P. falciparum* (in human) and *P. coatneyi* (in macaque) infections. **a** Heatmap of overlapping genes in *Macaca mulatta* (brainstem) versus *Homo sapiens* (blood). Created in BioRender. Malleret, B. (2025) <https://BioRender.com/6gfkww>. **b** Heatmap of overlapping genes in *Macaca mulatta* (brainstem) versus *Macaca mulatta* (blood). Created in BioRender. Malleret, B. (2025) <https://BioRender.com/6gfkww>. **c** Heatmap of overlapping genes in *Homo sapiens* (blood) versus *Macaca mulatta* (blood).

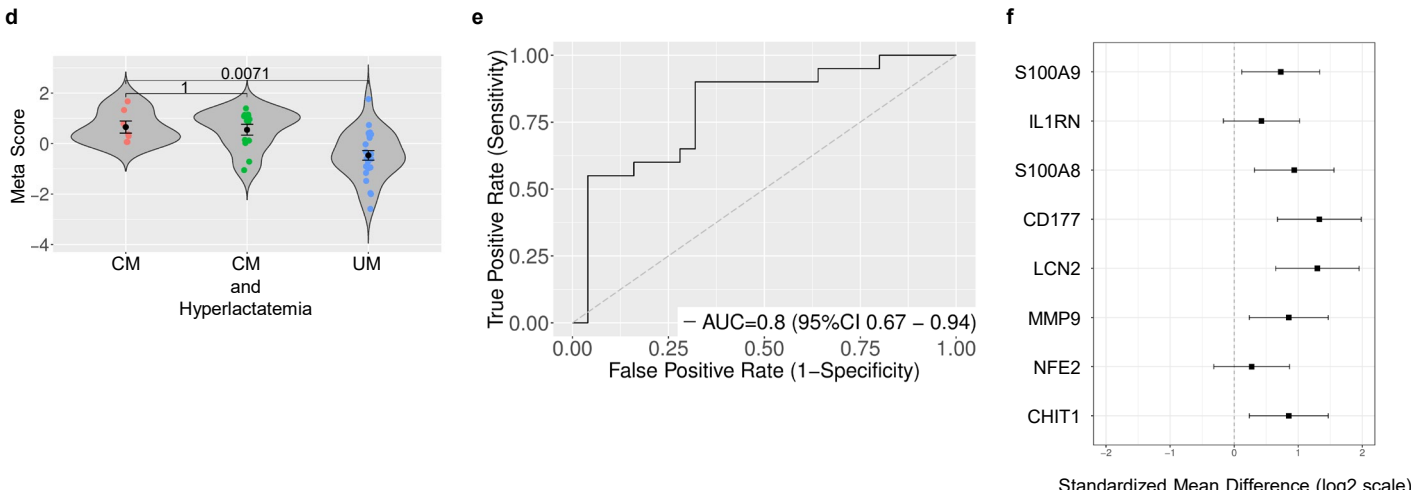


Supplementary Figure 5. Biomarkers of methylene blue treatment in macaque brainstem and human blood. Performance of an OPLS-DA model in discriminating between mild and cerebral malaria samples. The features of this model were the first three principal components of the 574 DEGs. Our 9 biomarkers were highlighted in red.

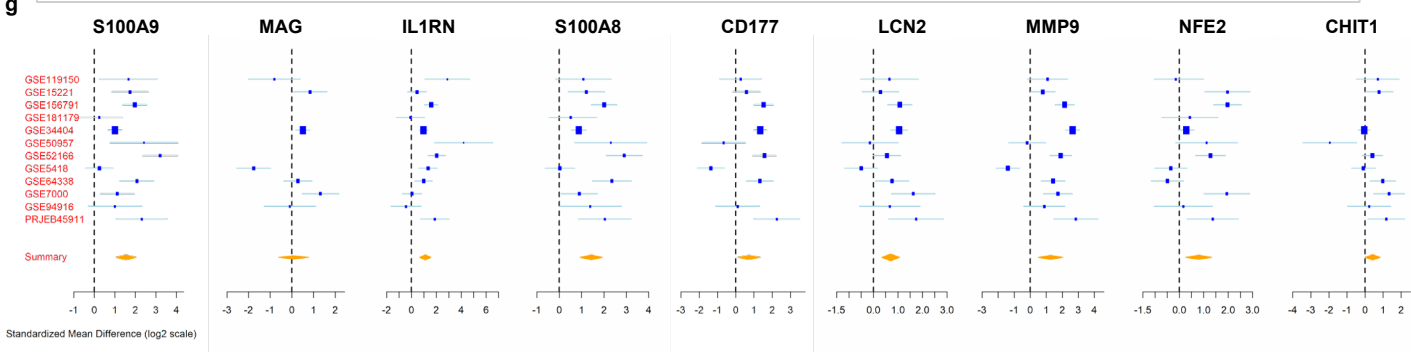
Cerebral vs. Uncomplicated Malaria RNA-seq datasets: GSE1124, GSE33811, GSE72058, GSE116306, GSE117613



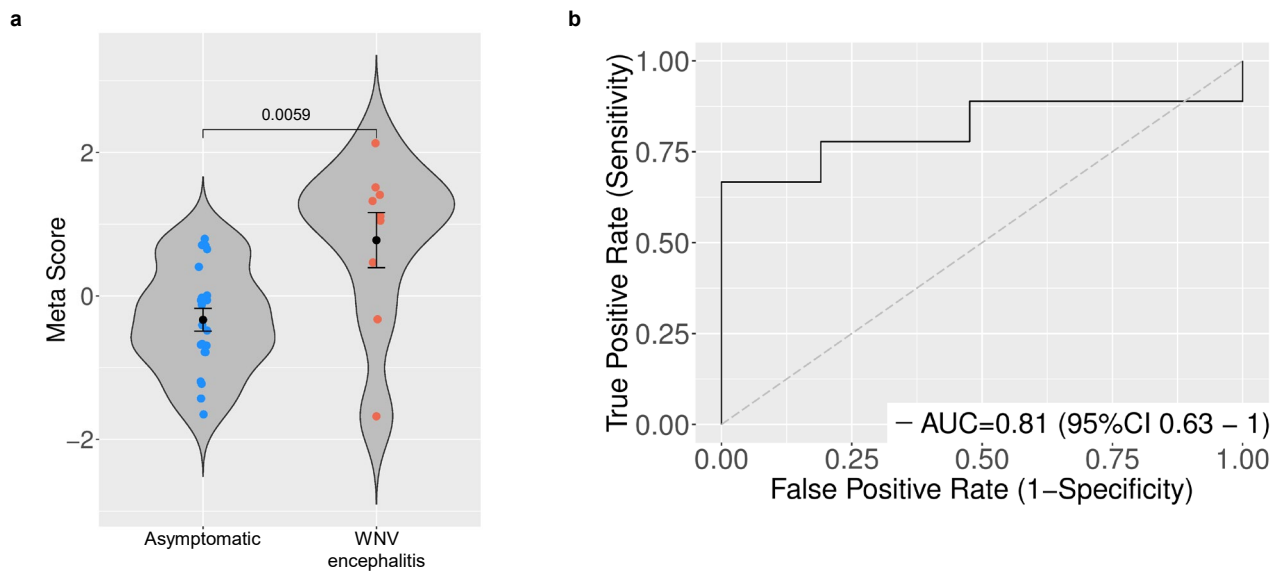
Cerebral vs. Uncomplicated Malaria MicroArray dataset: E-MTAB-6413



Uncomplicated Malaria vs. Healthy Controls RNA-seq datasets: GSE5418, GSE119150, GSE52166, GSE34404, GSE7000, GSE156791, GSE181179, GSE50957, GSE94916, GSE15221, GSE64338, PRJEB45911



Supplementary Figure 6. Nine candidate genes identified in the present study as blood biomarkers of cerebral malaria used with MetaIntegrator package¹ to analyze public gene expression datasets where human subjects were infected with *P. falciparum*. **a** Violin plot of the meta-scores of n=131 CM samples and n=59 UM samples derived from public microarray datasets GSE1124, GSE33811, GSE72058, GSE116306 and GSE117613, computed using the set of nine candidate biomarker genes. P-values comparing group means on the violin plots were computed using Wilcoxon rank sum test (two-sided). **b** Receiver operating characteristic (ROC) curve comparing CM vs. UM samples. The meta-scores were used for classifying samples as associated with CM or UM and the detection threshold was varied to generate the ROC curve. **c** Forest plot showing the standardized difference of mean in CM samples and UM samples of each candidate biomarker gene, computed as the log2-transformed Hedge's adjusted g value. The whiskers represent the 95% confidence interval. **d, e, f** Same analysis as above repeated on the public RNA-seq dataset E-MTAB-6413 (n=7, CM; n=13, CM and Hyperlactatemia; n=25, UM). **g** Forest plots for each of the nine candidate biomarker genes showing the standardized difference of mean in samples from n=246 individuals with UM and n=228 healthy controls, computed as the log2-transformed Hedge's adjusted g value. The whiskers represent the 95% confidence interval.



Supplementary Figure 7. Nine candidate genes identified in the present study as blood biomarkers of cerebral malaria used with MetaIntegrator package to analyze PBMC samples from the public gene expression dataset GSE46681 where human subjects were infected with the West Nile virus. **a** Violin plot of the meta-scores of n=21 asymptomatic and n=9 patients with encephalitis. **b** Receiver operating characteristic (ROC) curve for discriminating asymptomatic vs. encephalitis samples.